Nanoscale

Accepted Manuscript

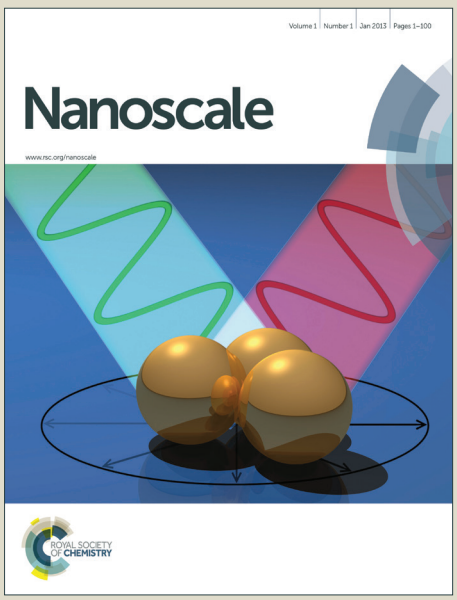

ROYAL SOCIETY OF CHEMISTRY

www.rsc.org/nanoscale

Nanoscale

Article

Graphene based tunable terahertz sensor with double Fano resonances

Received 00th January 20xx,
Accepted 00th January 20xx

DOI: 10.1039/x0xx00000x

www.rsc.org/

Yuping Zhang,[ab] Tongtong Li, [a] Beibei Zeng, [b*] Huiyun Zhang, [a] Huanhuan Lv, [a] Xiaoyan Huang, [a] Weili Zhang [c] and Abul K. Azad [b †]

We propose an ultrasensitive terahertz (THz) sensor consisting of a subwavelength graphene disk and an annular gold ring within a unit cell. The interference between the resonances arising from the graphene disk and the gold ring gives rise to Fano type resonances and enables ultrasensitive sensing. Our full wave electromagnetic simulations show frequency sensitivity as high as 1.9082THz/refractive index unit (RIU) and a figure of merit (FOM) of 6.5662. Furthermore, the sensing range can be actively tuned by adjusting the Fermi level of graphene.

1. Introduction

Fano resonances, originating from the coherent coupling and interference between discrete and continuous states, show a sharp and asymmetric line shape and have the ability to produce large electromagnetic field congregation.[1,2] Since Fedotov *et al*. first observed Fano resonances in metamaterials (MMs) composed of asymmetrical split ring arrays,[3] the Fano resonance characteristics in MMs and plasmonic nanostructures have attracted great interests in recent years.[4-21] There have been many potential applications of Fano resonances in biological and chemical sensors, active plasma switch, and slow light field.[22-26] Among these, sensing becomes the most critical application of Fano resonances at terahertz, infrared and optical frequencies,[27-32] due to their narrow linewidth and high quality (Q) factor, which are highly desirable for increasing the sensitivity of a sensor. Thus, it is promising to incorporate Fano resonances into traditional MMs [33] to enhance their sensing performances. Additionally, most of previous sensors employ static geometric design, therefore, once the device is fabricated their resonant wavelengths mostly remain fixed.

Graphene is a single-atom-thick and two-dimensional carbon material that has become the focus of research because of its remarkable electronic, mechanical, and thermal properties.[34,35] The tunable electromagnetic properties of graphene via manipulating its Fermi level by electrical gating or chemical doping enable tunable MMs devices.[36,37] So it would be intriguing to incorporate graphene in the MMs design to enable dynamically tunable Fano resonances for sensing applications.

In this paper, we numerically studied a tunable THz sensor with double Fano resonances, which utilizes a periodic array of unit cells consisting of a monolayer graphene disk located at the center of a gold ring. Double Fano resonances with narrow linewidth and high Q are excited by interferences between SPPs generated on the graphene disk and the gold ring. Under certain conditions the Q-factor of our resonator can be as high as 59. Besides, the double Fano resonances in our designed resonator exhibit different sensing sensitivities (frequency sensitivity 1.4439THz/RIU and 1.9082THz/RIU for mode A and B, respectively) and figure-of-merit (FOM) (6.5662 and 2.7812 for mode A and B, respectively), when the analyte thickness is set to 0.24μm, which can be potentially used to differentiate bulk/surface effects[32,38] in the terahertz region. Furthermore, our proposed double Fano resonances can be actively tuned by adjusting the gate voltage to the graphene layer.

2. Structural design and physical mechanism

The top and cross-sectional views of the double Fano resonator structure under consideration are shown in Figs. 1(a) and (b), respectively. The unit cell is composed of a circular disk of monolayer graphene positioned at the center of an circular gold ring deposited on top of a SiO_2 substrate with a relative permittivity $\varepsilon_s = 3.5$. The unit cells are arranged in a periodic array with a square lattice with a lattice parameter P = 8μm. The outer radius R_m and width W of gold ring are 3.5 μm and 0.1μm, respectively. The thicknesses of the gold film and the dielectric substrate are t_m = 0.03μm and t_s = 1μm, respectively. The graphene disk has a thickness t_g=0.5nm and

[a] Qingdao Key Laboratory of Terahertz Technology, College of Electronic Communication and Physics, Shandong University of Science and Technology, Qingdao 266510，China.
[b] MPA-CINT, MS K771, Los Alamos National Laboratory, Los Alamos, New Mexico 87545, USA.
[c] School of Electrical Engineering and Computer Science, Oklahoma State University, Stillwater, Oklahoma 87074, USA.
* Email: beibei@lanl.gov
† Email: aazad@lanl.gov

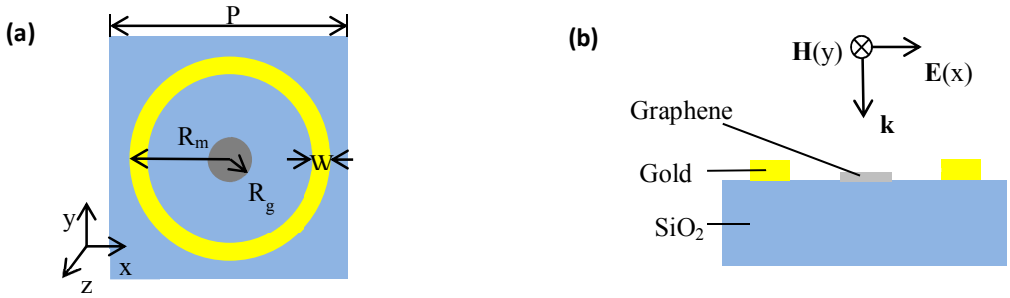

Fig.1 (a) Top view and (b) cross-sectional view of the unit cell with a normally incident plane wave.

radius R_g=0.75μm. The proposed Fano resonances are excited by the electric field of a normally incident terahertz plane wave propagating in the z direction.

At low terahertz frequencies, the surface conductivity of graphene is dominated by the intraband contribution and can be approximated by a Drude model as[39]

$$\sigma \approx j\frac{e^2 E_F}{\pi\hbar(\hbar\omega + j\Gamma)} \quad . \tag{1}$$

where ω is the angular frequency, $\hbar$ is the reduced Planck constant, and E_F is Fermi level energy of graphene. Γ is the damping constant which can be given by $-(e\hbar v_f^2)/(\mu E_F)$, where $v_f = 10^6 m/s$ is the Fermi velocity and $\mu = 10{,}000 cm^2/Vs$ is the graphene's electron mobility[40]. The permittivity of graphene can be obtained by the following equation

$$\varepsilon_r(\omega) = 1 + j\frac{\sigma}{t_g \epsilon_0 \omega} \quad . \tag{2}$$

Since the general expression of permittivity in Drude model is

$$\varepsilon(\omega) = 1 - \frac{\omega_{P,G}^2}{\omega(\omega + j\Gamma/\hbar)} \quad , \tag{3}$$

one can calculate the plasma frequency of graphene layer by comparing the equations (2) and (3) as[41]

$$\omega_{P,G} = \sqrt{\frac{e^2 E_F}{t_g \epsilon_0 \pi \hbar^2}} \quad . \tag{4}$$

To obtain high sensitivity, we have deliberately chosen the thickness of gold ring to t_m = 30nm, which is about one skin depth thick at our operating frequencies, and is capable of supporting plasmonic resonances[42]. Also, within the THz frequencies, 30 nm is thick enough to incorporate the bulk parameters of gold for calculating dielectric properties using Drude model[43]. In our simulation, we used Drude formula to model the gold film with plasma frequency $\omega_P = 1.37 \times 10^{16} rad/s$ and collision frequency $\omega_c = 6.2818 \times 10^{12}/s$[44].

The Fano resonator is simulated using the commercial full-wave EM simulation software CST Microwave Studio. We set the perfect electric boundary and perfect magnetic boundary in the x and y directions, respectively. An open boundary condition is set along the z direction. Fig. 2(a) shows the simulated amplitude transmission spectra of three MMs composed of the gold ring only (black), the graphene disk only

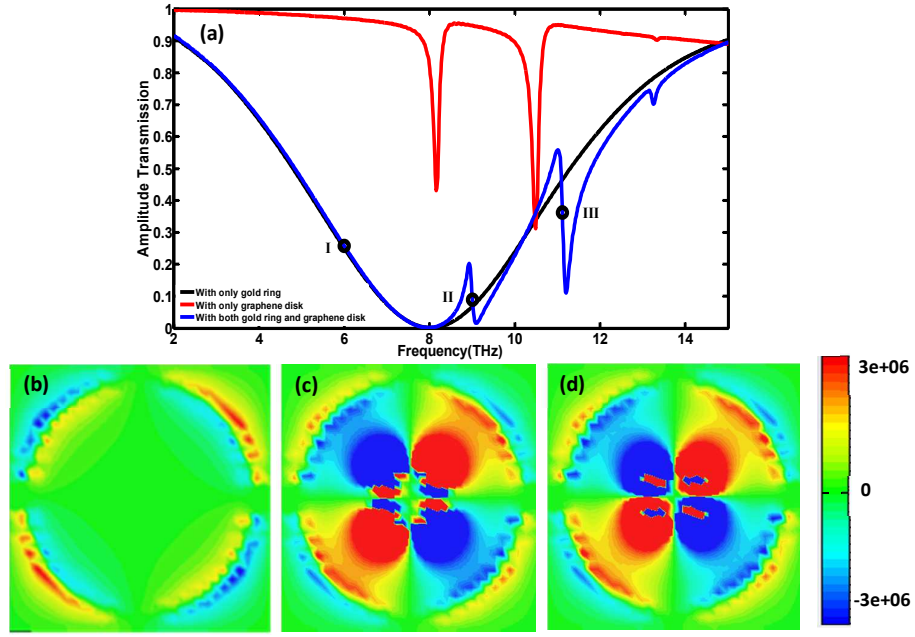

Fig. 2 (a) Terahertz amplitude transmission spectra through MMs composed of gold rings only (black) and graphene disks only (red) and both the gold ring and the graphene disk (blue) with the Fermi level of graphene fixed at 1.5eV. Electric field distributions on the unit cell simulated at frequency points I, II, and III, corresponding to the frequencies: (b) 6.000THz, (c) 9.007THz, and (d) 11.117THz, respectively.

(red), and the combination of gold rings with graphene disks (blue) with the Fermi level of 1.5eV that could be realized by doping. When excited with an incident wave, the circular gold ring and the circular graphene disk can support their own SPPs. Through the careful structural design one can overlap the resonances of the gold ring and the graphene disk to excite Fano resonances through the coupling between the modes excited in gold rings and graphene disk. As shown in Fig.2(a), the SPP mode excited in the gold ring has a much broader line width compared to the resonance excited in the graphene disk. The combined structure (ring + disk) exhibits the Fano-like line-shapes due to the interference between the independent resonances arising from the gold ring and the graphene disk.

The nature of the different modes is represented in Fig.2(b), (c) and (d) with electric field distributions at three frequency points I, II, and III, corresponding to the frequencies: 6.000THz, 9.007THz and 11.117THz, respectively. As demonstrated in the figure, the electric field induced from the gold ring is dominant at point I, which does not spectrally overlap with the resonance of the graphene disk. The field distribution at point I is similar to the field distribution of only gold ring (not shown here). At point II and III, the electric field distribution displays that the SPP modes generated in the gold ring and graphene disk interfere strongly at these two frequency points.

3. Sensing performance of the double Fano resonances

To investigate the sensitivity of our proposed sensor based on Fano resonances, we apply an analyte layer on the top of the device. The thickness and refractive index of the analyte are t_a and n, respectively. First, the influence of analyte thickness on the response of the Fano resonator is investigated. For this set of simulations, we fix the Fermi level of the graphene disk and the refractive index of the analyte to 1.5eV and 1.43 (PTFE), respectively. Fig.3(a) depicts the amplitude transmission spectra of the Fano resonator computed for each value of the thickness t_a of the analyte. As the thickness of the analyte increases from 0.06μm to 0.24μm in step of 0.06 μm, the resonant frequencies of both mode A and mode B show a monotonous red-shift due to the increase in the effective dielectric constant of the top layer and their amplitude at resonance decrease slightly. The frequency shifts of mode A and B are 0.403THz and 0.546THz, with corresponding amplitude modulations of 4.63% and 4.35%, respectively. The rate of amplitude modulation of mode A is higher than that of mode B whereas the resonant frequency shift of mode B is higher than that of the mode A. An increase in the calculated Q factor is also observed with the analyte thickness due to the increase in the capacitance associated with the Fano resonators. The Q factors of mode A and mode B are 59 and 24 for the analyte thickness of 0.24μm.

Next, we investigate the amplitude transmission spectra versus frequency with different refractive indices of the analyte. The simulated results are shown in Fig.3(b) for the analyte thickness t_a=0.06 μm and the Fermi level E_F=1.5eV,

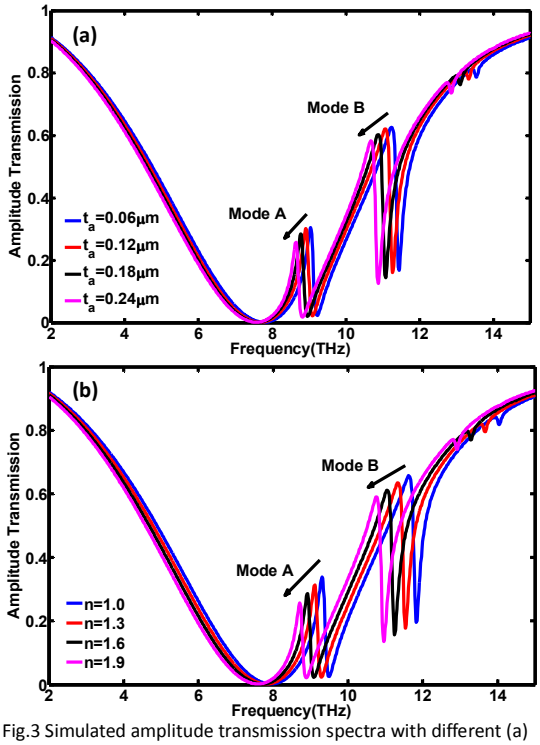

Fig.3 Simulated amplitude transmission spectra with different (a) thicknesses and (b) refractive indices of the analyte placed on the top of the device.

respectively. The resonant frequencies of both mode A and mode B red-shift while the refractive index of the analyte increases from 1.0 to 1.9 in a step of 0.3. The total shifts in resonant frequency of mode A and mode B are 0.598THz and 0.858THz, respectively. In addition, the amplitude transmission slightly decreases with the increasing refractive index because of the mismatching of indices at the interface. The corresponding amplitude modulation of mode A is 8.09% and that of mode B is 6.69%. The range of refractive index represents a set of technologically important materials for terahertz sensing applications. For example, our mid-range of index represents the refractive index of PTFE (n=1.43), a material frequently used as the binder with many explosives such as TNT (n=1.76), RDX (n=1.66), and HMX (n=1.81). The range also covers biological materials such as air-dried Herring DNA (n≈1.65) and Ovalbumin (n≈1.15)[45].

Since the variations in mode A and mode B of double Fano resonator are different for an identical thickness of analyte over-layer, we investigate the sensitivity of both resonances by changing the refractive index for the same analyte thickness. First, we calculate and plot the frequency shift and amplitude modulation as a function of the refractive index of the analyte for a fixed thickness of 0.06μm as shown in Fig.4(a). The shifts in the resonant frequency for both modes increase linearly with the refractive index of the analyte. However, the slope of linear shift of mode B is greater than that of the mode A, meaning that the mode B has higher frequency sensitivity. The slope also represents the frequency sensitivity. The estimated frequency sensitivity of mode A and B are 0.65THz/RIU and 0.9518THz/RIU, respectively. The amplitude modulations of

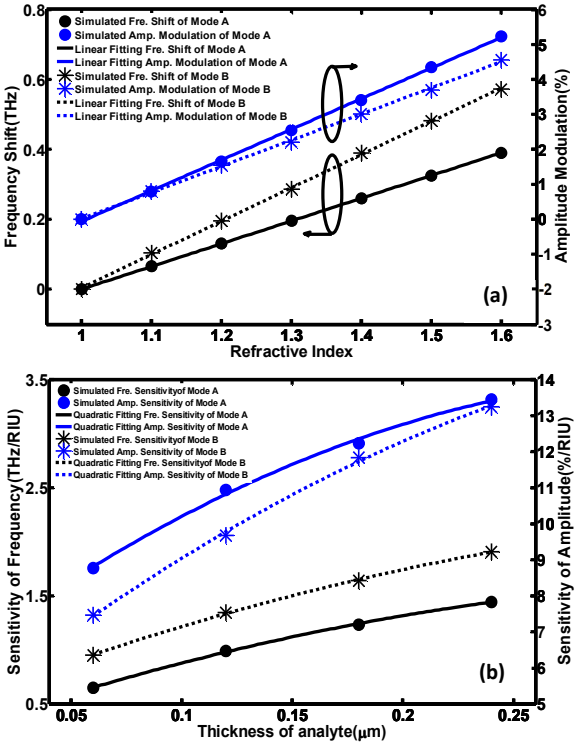

Fig.4 (a) Frequency shift and amplitude modulation versus the refractive index of the analyte located on the surface of device for a fixed thickness of 0.06μm. (b) Sensitivity of frequency and amplitude versus the thickness of the analyte of both mode A and mode B.

mode A and mode B as a function of refractive index are also shown in fig. 4(a). Our amplitude modulations of both modes increase linearly with the refractive index. Furthermore, we can also calculate the amplitude sensitivities of both resonances by using the slope of the fitted line of amplitude transmission. The calculated amplitude sensitivities of mode A and mode B are 8.7%/RIU and 7.4714%/RIU, respectively.

We then investigate the effect of different thickness of analyte on the sensitivity of mode A and mode B. As shown in Fig. 4(b), the frequency sensitivities of both resonances increase while the thickness of the analyte is increased from 0.06μm to 0.24μm. The frequency sensitivity increases for both resonant modes can be represented by quadratic fitting curves, indicating that they may saturate at a thickness larger than 0.24μm. The calculated frequency sensitivities of mode A and B are 1.4439THz/RIU and 1.9082THz/RIU, respectively, for an analyte thickness of 0.24μm. Mode B shows higher frequency sensitivity than that of mode A at any given analyte thickness. Fig. 4(b) also shows the amplitude sensitivity of both resonances due to the change in analyte thickness. The sensitivity of amplitude increases quadratically with the thickness of the analyte. The amplitude sensitivity of mode A is higher than that of mode B, and both of them have the tendency to saturate as the analyte becomes thicker.

Fig. 5 represents the evolution of the full width at half maximum (FWHM) and the corresponding FOM for both resonant modes as a function of the refractive indices of

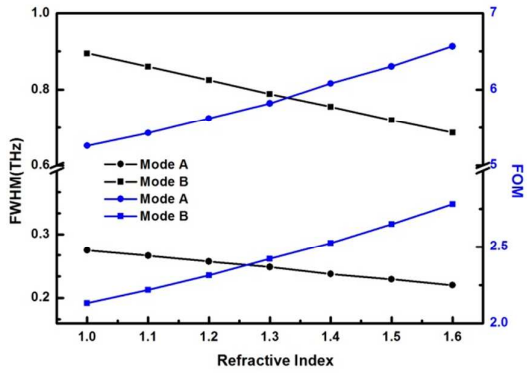

Fig.5 FWHM and FOM of mode A and mode B in response to different refractive indices of the analyte.

analyte with a fixed thickness of 0.24μm. The FWHM of both mode A and B decrease almost linearly from 0.2745THz to 0.2199THz, and from 0.895THz to 0.6861THz, respectively, with the increase of the refractive index of the analyte. Therefore, the FOM values increases almost linearly. The FOM of mode A increases from 5.2601 to 6.5662 while that of mode B increases from 2.1321 to 2.7812. The FOM of mode A is higher than mode B by 57.64%, which indicates that the resonance of mode A has a smaller rate of energy dissipation compared to mode B.

To clarify the sensing mechanism of Fano resonator, we analyze the electric field distribution of both modes A and B with and without the analyte. The simulations are performed under the condition that the thickness and refractive index of the analyte are fixed at 0.06μm and 1.4, respectively, and the Fermi level of the graphene disk is fixed at 1.5eV. The resonant frequencies of mode A and B are 9.046THz and 11.23THz, respectively. A comparison of Fig.6 (a) and (b) shows strong field enhancement between the graphene disk and the gold ring in the presence of analyte at 9.046THz. We also observe changes in electric field distribution at the edge of graphene disk and gold ring due to the strong coupling between them. Fig.6(c) and (d) displays the electric field distribution at the resonant frequency 11.23THz of mode B without and with

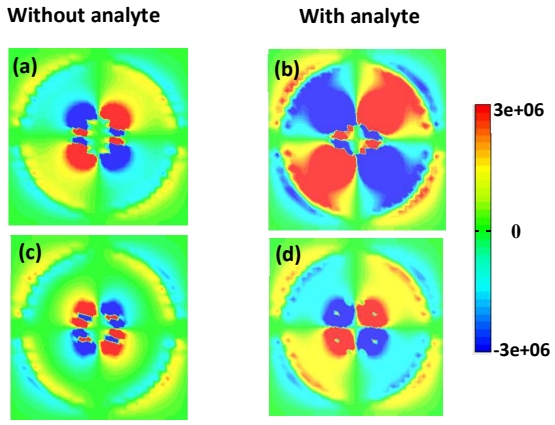

Fig.6 Electric field distribution of resonance frequency at (a,c)9.046THz for mode A and (b,d)11.23THz for mode B.

analyte, respectively. At this frequency the field distribution around the graphene disk shows a phase change of the electric field in the presence of analyte. We believe that the presence of the analyte changes the interference condition, leading to redistribution of electric and magnetic fields.

Finally, to analyze the tunable property of the double Fano resonator structure, we simulate the frequency dependent amplitude transmission for various Fermi levels of graphene. The simulated results are shown in Fig. 7(a) for an analyte of thickness t_a = 0.06 μm and refractive index n = 1.43. While the Fermi level of graphene was varied from 1.2ev to 1.8ev in step of 0.2ev, both resonant modes showed blue-shifts in their resonant frequencies, with its frequency tuning range for mode A and B starting from 8.149THz and 10.099THz, respectively. The frequency shifts of mode A and mode B are 1.703THz and 2.171THz, respectively, for the Fermi level changes from 1.2ev to 1.8ev. In addition to the change in the resonant frequencies we also observed amplitude modulations. The amplitude modulation of mode A and B are 48.2% and 39.51%, respectively, for the corresponding change of the Fermi level. The modulation of Fano resonances is attributed to the Fermi level induced change in the graphene properties. The independent resonances excited in a graphene disk show blue-shifts and enhancement in the resonant amplitudes with increasing Fermi level. These changes in the graphene resonators ultimately influence the tuning ranges of Fano resonances. To realize the Fano resonances with a lower Fermi energy (e.g., 0.9eV ~ 1.2eV), we have redefined our gold ring with an outer radius R_m = 3.9 μm, period 8μm, radius of graphene disk R_g = 0.825μm, while keep other parameters unchanged. Fig. 7(b) shows the tuning of resonant frequencies of mode A and mode B as a function of E_F, with its tuning range starting from 6.856 THz and 8.578 THz for mode A and B, respectively. Our simulation indicates (not shown here) that the graphene disk exhibits very weak resonance for a Fermi level lower than 0.9eV, therefore, it is difficult to obtain the Fano resonances when Fermi energy is below 0.9eV.

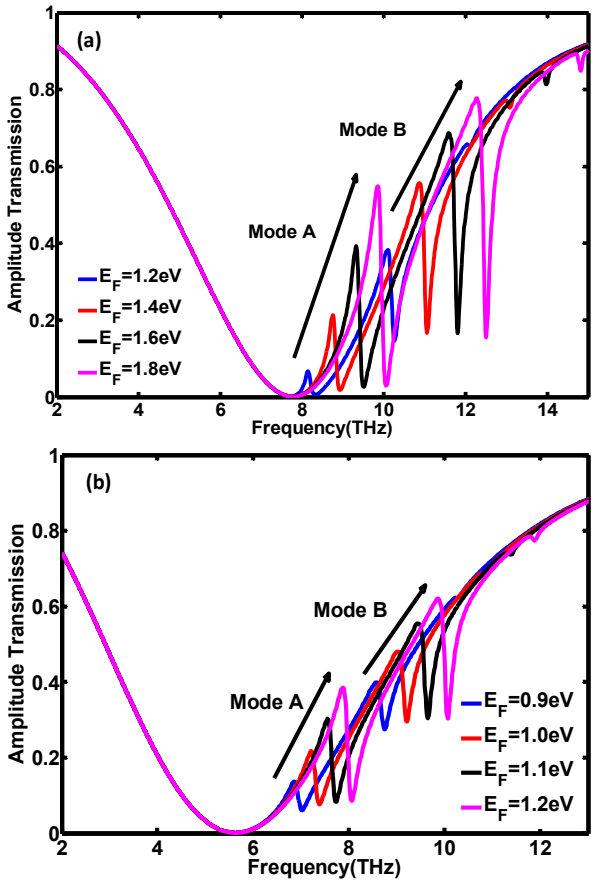

Fig.7 Simulated amplitude transmission spectra of the (a) structure with same parameters as used in fig. 2 with Fermi level changes from 1.2eV to 1.8eV; (b) structure with redefined parameters (R_m = 3.9 μm, P = 8μm, R_g = 0.825μm, and other parameters unchanged), with Fermi level changes from 0.9eV to 1.2eV.

4. Conclusions

In summary, we have demonstrated a tunable ultrasensitive THz sensor with double Fano resonances, which result from interferences between the SPPs of gold ring and graphene disk. The influence of thickness and refractive index of analyte on the frequency and amplitude sensitivities are studied in detail. Numerical results show that a high frequency sensitivity of 1.908THz/refractive index unit (RIU) for mode B and a figure of merit (FOM) of 6.5662 for mode A can be obtained simultaneously using our proposed structure with double Fano resonances. The introduction of graphene in this sensor makes the sensing range actively tunable. The proposed structure can be realized using current micro/nano fabrication facilities, which may open up a new path for sensing in the THz frequencies.

Acknowledgements

We acknowledge partial support from the Los Alamos National Laboratory LDRD program. This work was performed, in part, at the Center for Integrated Nanotechnologies, a U.S. Department of Energy, Office of Basic Energy Sciences under Contract No. DE-AC52-06NA25396. It was also partially supported by the Natural Science Foundation of Shandong Province, China (Grant No. ZR2012FM011), Qingdao city innovative leading talent plan(13-CX-25), the CAEP THz Science and Technology Foundation (Grant No.201401), Qingdao Economic & Technical Development Zone Science & Technology Project (Grant No.2013-1-64), and the Shandong University of Science and Technology Foundation, China (Grant No. YC140108)

Notes and references

1 U. Fano, *Phys. Rev.*, 1961, **124**, 1866.
2 W. Ding, B. Luk'Yanchuk and C. W. Qiu, *Phys. Rev. A*, 2012, **85**,025806.
3 V. A. Fedotov, M. Rose, S. L. Prosvirnin, N. Papasimakis and N. I. Zheludev, *Phys. Rev. Lett.*, 2007, **99**, 147401.

4 O. Peña-Rodríguez, U. Pal, M. Campoy-Quiles, L. Rodriguez-Fernández, M. Garriga and M. I. Alonso, J. *Phys. Chem. C*, 2011, **115**, 6410.
5 F. Hao, P. Nordlander, Y. Sonnefraud, P. V. Dorpr and S. A. Maier, *Acs Nano*, 2009, **3**, 643.
6 D. J. Wu, S. M. Jiang and X. J. Liu, *J. Chem. Phys.*, 2012, **136**, 034502.
7 J. A. Fan, K. Bao, C. Wu,J. Bao, R. Bardhan, N. J. Halas, V. N. Manojaran, G. Shvets, P. Nordlander and F. Capasso , *Nano Lett.*, 2010, **10**, 4680.
8 M. R. Shcherbakov, M. I. Dobynde, T. V. Dolgova, D. P. Tsai and A. A. Fedyanin, *Phys. Rev. B*, 2010, **82**, 193402.
9 H. Liu, X. Wu, B. Li, C. Xu, G. Zhang and L. Zheng, *Appl. Phys. Lett.*, 2012, **100**, 153114.
10 O. Peña-Rodríguez, A. Rivera, M. Campoy-Quiles and U. Pal, *Nanoscale*, 2013, **5**, 209.
11 B. Seo, K. Kim, S. G. Kim, A. Kim, H. Cho and E. Choi, *J. Appl. Phys.*, 2012, **111**,113106.
12 N. Soltani, É. Lheurette and D. Lippens, *J. Appl. Phys.*, 2012, **112**, 124509.
13 T. Cao, C. Wei, R. E. Simpson, L. Zhang and M. J. Cryan, *Opt. Mater. Express*, 2014, **4**, 1775.
14 B. Yun, G. Hu, J. Cong and Y. Cui, *Plasmonics*, 2014, **9**, 691.
15 J. Wang, C. Fan, J. He, P. Ding, E. Liang and Q. Xue, *Opt. Express*, 2013, **21**, 2236.
16 K. Wen, Y. Hu, L. Chen, J. Zhou, L. Lei and Z. Guo, *Plasmonics*, 2015, **10**, 27.
17 Y. U. Lee, E. Y. Choi, E. S. Kim, J. H. Woo, B. Kang, J. Kim, B. C. Park, T. Y. Hong, J. H. Kim and J. W. Wu, *J. Opt.*, 2015, **17**, 025103.
18 L. Y. Yin, Y. H. Huang, X. Wang, S. T. Ning and S. D. Liu, *AIP Adv.*, 2014, **4**, 077113.
19 T. Cao, L. Zhang, Z. P. Xiao and H. Huang, *J. Phys. D,* 2013, **46**, 395103.
20 T. Cao and L. Zhang, *Opt. Express*, 2013, **21**, 19228.
21 R. Singh, W. Cao, I. Al-Naib, L. Cong, W. Withayachumnankul and W. Zhang, *Appl. Phys. Lett.*, 2014, **105**, 171101.
22 A. E. Miroshnichenko, S. Flach and Y. S. Kivshar. *Rev. Mod. Phys.*, 2010, **82**, 2257.
23 S. D. Liu, Z. Yang, R. P. Liu and X. Y. Li, *J. Phys. Chem. C*, 2011, **115**, 24469.
24 W. S. Chang, J. B. Lassiter, P. Swanglap, H. Sobhani, S. Khatua, P. Nordlanser, N. J. Halas and S. Link, *Nano Lett.*, 2012, **12**, 4977.
25 X. Piao, S. Yu and N. Park *Opt. Express*, 2012, **20**, 18994.
26 C. Wu, A. B. Khanikaev, G. Shvets *Phys. Rev. Lett.*, 2011, **106**, 107403.
27 N. Liu, M. L. Tang, M. Hentschel, H. Giessen and A. P. Aiviastos, *Nat. Mater.*, 2011, **10**, 631.
28 J. Zhao, C. Zhang, P. V. Braun and H. Giessen, *Adv. Mater.*, 2012, **24**,OP247.
29 Y. Yang, I. I. Kravchenko, D. P. Briggsand J. Valentine, arXiv preprint arXiv: 1405.3901, 2014.
30 B. Ng, S. M. Hanham, V. Giannini, Z. C. Chen, M. Tang, Y. F. Liew, N. Klein, M. h. Hong and S. A. Maier, *Opt. Express*, 2011, **19**,14653.
31 H. Tao, L. R. Chieffo, M. A. Brenckle, S. M. Siebert, M. L, A. C. Strikwerda, K. Fan, D. L. Kaplan, X. Zhang, R. D. Averitt and F. G. Omenetto, *Adv. Mater.*, 2011, **23**, 3197.
32 B. Zeng, Y. Gao and F. J. Bartoli, *Appl. Phys. Lett.*, 2014, **105**, 161106
33 H. Tao, A. C. Strikwerda, M. Liu, J. P. Mondia, E. Ekmekci, K, Fan, D. L. Kaplan, W. J. Padilla, X. Zhang, R. D. Averitt and F. G. Omenetto, *Appl. Phys. Lett.*, 2010, **97**, 261909.
34 K. S. Novoselov, V. I. Fal, L. Colombo, P. R. Gellert, M. G. Schwab and K. Kim, *Nature*, 2012, **490**, 192.
35 A. K. Geim, *Science*, 2009, **324**, 1530.
36 X. He, Z. Y. Zhao and W. Shi, *Opt. Lett.*, 2015, **40**, 178.
37 X. He, *Carbon*, 2015, **82**, 229.
38 B. Zeng, Y. Gao and F. J. Bartoli, Nanoscale, 2015, **7**, 166.
39 G. W. Hanson, J. *Appl. Phys.*, 2008, **103**, 064302.
40 L. Wang, X. Chen, A. Yu, Y. Zhang, J. Ding, and W. L, *Sci. Rep.*, 2014, **4.**
41 M. Amin, M. Farhat and H. Bağcı, *Sci. Rep.*, 2013, **3**.
42 R. Singh, E. Smirnova, A. J. Taylor, J. F. O'Hara and W. Zhang, *Opt. Express, 2008, **16**, 6537.*
43 M. Walther, D. G. Cooke, C. Sherstan, M. Hajar, M. R. Freeman and F. A. Hegmann, *Phys. Rev. B, 2007*, **76**, 125408.
44 M. A. Ordal, L. L. Long, R. J. Bell, S. E. Bell, R. R. Bell, R. W. Alexander, C. A. Ward, *Appl. Opt.* 1983, **22**, 1099.
45 T. Globus, R. Parthasarathy, T. Khromova, D. Woolard, N. Swami, A. J. Gatesman, and J. Waldman, *Proc. SPIE,* 2004, **5584**, 1.